Int. J. Electrochem. Sci., 17 **(2022)** Article Number: 220929, doi: 10.20964/2022.09.10

International Journal of
ELECTROCHEMICAL
SCIENCE
www.electrochemsci.org

Synthesis of TiO_2/g-C_3N_4 Hybrid Photocatalyst and its Application for Degradation of Chlorophenol as Organic Water Pollutant

Nianping Chi[*], *Wenzhen Xu*

School of Municipal and Geomatics Engineering, Hunan City University, Hunan Province Engineering ＆Technology Research Center for Rural Water Quality Safety, Yiyang, Hunan 413000, China
[*]E-mail: cnp2022zjgsdx@163.com

Received: 24 April 2022 / *Accepted:* 16 June 2022 / *Published:* 7 August 2022

This study used a hydrothermal-calcination approach to make TiO_2/g-C_3N_4 hybrid photocatalysts, which were then used to degrade 2-Chlorophenol (2-CP) as organic water pollutants under solar irradiation. According to XRD and SEM studies, the high porosity TiO_2/g-C_3N_4 hybrid nanocatalyst was successfully synthesized. The band gap energies of g-C_3N_4, TiO_2, and TiO_2/g-C_3N_4 hybrid nanocatalysts were 2.58, 2.88, and 3.16 eV, respectively, according to optical studies. The decrease in band gap energy in TiO_2/g-C_3N_4 hybrid toward TiO_2 was evidence of facilitation in photo-excitation of charge carries using low energy, which can extend the light absorption spectrum into visible regions and holes and accelerate the transmission of the photogenerated charge carriers. Electrochemical analysis revealed that the TiO_2/g-C_3N_4 hybrid had a lower charge transfer resistance and a longer electron life time than pure g-C_3N_4 and TiO_2, signifying a low electron recombination rate, allowing for faster electron transport and higher photodegradation efficiency. The entire degradation of 100 ml of 25 mg/L 2-CP was obtained after 125, 110, and 65 minutes of sun irradiation, respectively, in the presence of g-C_3N_4, TiO_2, and TiO_2/g-C_3N_4 hybrid nanocatalysts. The practical application of a TiO_2/g-C_3N_4 hybrid nanocatalyst to treat 2-CP in genuine industrial wastewater samples was investigated, and the results revealed the produced photocatalyst's excellent effectiveness in treating 2-CP in industrial wastewater.

Keywords: Photocatalyst; Photodegradation; TiO_2/g-C_3N_4 hybrid; 2-Chlorophenol; Industrial wastewater

1. INTRODUCTION

Chlorophenols (CPs) are a class of compounds formed when phenol is electrophilically halogenated with chlorine [1, 2]. In businesses and goods, CPs are used to make insecticides, herbicides, medicines, and dyes. Some are used to kill algae and fungi as well as disinfect. Historically,

the compounds have been employed to preserve textile and leather products during storage and transportation [3, 4].

Industrial waste, herbicides, and insecticides, as well as the degradation of complex chlorinated hydrocarbons, all contribute to the proliferation of CPs as persistent and recalcitrant toxicants in the environment [5, 6]. The compounds are caustic and highly irritating or poisonous, and using respirators incorrectly can be deadly [7]. These substances are caustic and extremely irritating or poisonous [8]. CPs do not breakdown spontaneously and can easily accumulate in organs, tissues, and cells through food chains [9]. As a result, it is causing acute and chronic toxic effects on aquatic creatures, as well as the possibility of histopathological alterations, mutagenic, and carcinogenic effects [10, 11]. 2-Chlorophenol (2-CP), sometimes known as ortho-chlorophenol, is an organic chemical that is a phenol derivative. Disinfectants and insecticides containing related chemicals are utilized [12].

Many methods such as chemical and electrochemical oxidation [13], adsorption [14], ozonation [15], coagulation [16], Fenton and electro-Fenton oxidation [17-19], bacterial degradation [20], sonochemical [21, 22] and photocatalytic degradation [23-27] have been employed for the treatment of CPs contaminated wastewater. The photocatalytic degradation process is an interesting solution for the removal of organic water contaminants because it is both environmentally beneficial and affordable. As a result of this research, a TiO_2/g-C_3N_4 hybrid photocatalyst was synthesized utilizing a hydrothermal-calcination process and was used to degrade 2-CP as an organic water pollutant.

2. EXPERIMENT

2.1. Synthesis of TiO_2,g-C_3N_4 and TiO_2/g-C_3N_4 hybrid nanocatalysts

TiO_2/g-C_3N_4 hybrid nanocatalysts were synthesized using the hydrothermal-calcination technique [28]. In a nutshell, a dispersed aqueous mixture of 10 g/L melamine (99%, Sigma-Aldrich) and 10 g/L NH4F (≥98%) was ultrasonically created in an equal volume ratio. After that, 50 mL of the mixture was poured into 100mL Teflon-line autoclave and covered with a titanium foil (99.99%, 40mm x 30mm x 0.5mm, Sigma-Aldrich) that was vertically placed in the autoclave. The reaction was carried out at 160° C for 72 hours. After that, the product was collected and rinsed with deionized water before being heated for 5 hours at 530°C in a muffle furnace at a rate of 20 °C/min. For synthesis of the pure TiO_2, the above hydrothermal-calcination process was repeated without adding melamine and NH_4F, and for synthesis of the pure g-C_3N_4, the same process was performed without titanium foil.

2.2. Characterization

The crystal structures and morphology of the produced nanocatalysts were studied using an X-ray diffractometer (XRD; Rigaku D/max-2400, Japan) and scanning electron microscopy (SEM). A UV-vis spectrophotometer was utilized to detect optical absorption spectra (Model Omega 10, Bruins Instruments,Puchheim, FRG). Electrochemical impedance spectroscopy (EIS) measurements were performed under visible-light illumination, for comparing electron-transfer rates in photocatalysts at a frequency range of 10^{-1} to10^{6} Hz and 10mV AC voltage into 0.5M Na_2SO_4 solution (≥98%) by

potentiostat/galvanostat equipped with an electrochemical cell containing nanocatalysts modified fluorine doped tin oxide (FTO, Sigma-Aldrich) as working electrode, a Pt plate as counter,and Ag/AgCl as reference electrode. The obtained EIS data were fitted with an appropriate equivalent circuit using the software Z-view.

2.3. Study the photocatalytic Activity

The photodegradation activity of TiO_2,g-C_3N_4 and TiO_2/g-C_3N_4 hybrid nanocatalysts was evaluated for the treatment of 100 ml of 2-CP solution under solar illumination. The experiments were conducted on a reactor system consisted of a cylindrical Pyrex-glass cell with a 1000 mL capacity and a Philips tungsten-halogen lamp (250 W) was placed in a 8 cm just above the sample in the reactor. The mixture of 20 mg of nanocatalysts in 100 ml of prepared 2-CP solution with deionized water, as well as a prepared real sample of industrial wastewater. Before the photodegradation measurements, the mixture was magnetically stirred for one hour in a dark place to get an adsorption/desorption equilibrium between 2-CP molecules and the nanocatalysts. For photocatalytic experiments, the light source was irradiated on samples for a regular time interval, and irradiated samples were centrifuged at 10000 rpm for 8 minutes, filtered through a 0.22 µm membrane (MF-Millipore™, Merck, Germany) and collected. The concentration of 2-CP of the supernatants was measured by UV-vis absorbance (spectrophotometer, Bruins Instruments) at λ_{max} = 275 nm [29]. The 2-CP concentration corresponded to the absorbance intensity, which was used for the calculation of the degradation efficiency (η) by the following equation [26, 30]:

$$\eta\ (\%) = \frac{I_0 - I_t}{I_0} \times 100 = \frac{C_0 - C_t}{C_0} \times 100 \qquad (1)$$

Where I_o and I_t are absorbance intensity of initial and illuminated 2-CP solutions, respectively, and C_o and C_t is corresponded 2-CP concentration in initial and illuminated 2-CP solutions, respectively.

3. RESULTS AND DISCUSSION

3.1. Study of morphology and structure of nanocatalysts

Figure 1 shows XRD patterns of powders of g-C_3N_4, TiO_2, and TiO_2/g-C_3N_4 hybrid nanocatalysts. The (100) and (002) planes in g-C_3N_4 are related to the in-plane structure of tris-triazine units and the interlayer stacking of conjugated aromatic systems, respectively, in the XRD pattern [31-33]. According to the XRD patterns of TiO_2 and TiO_2/g-C_3N_4 hybrid, there are diffraction peaks at 25.20°, 37.75°, 47.97°, 53.68°, 54.191°, and 62.65°, which correspond to the typical crystal facet of anatase TiO_2 with (101), (004),(200), (105), (211),and (204) planes, respectively (JCPDS card no. 21-1272) [34, 35]. However, the TiO_2/g-C_3N_4 hybrid nanocatalyst diffraction peaks show an additional peak of (002) plane of g-C_3N_4, indicating the TiO_2/g-C_3N_4 hybrid nanocatalyst was successfully synthesized by the hydrothermal-calcination method.

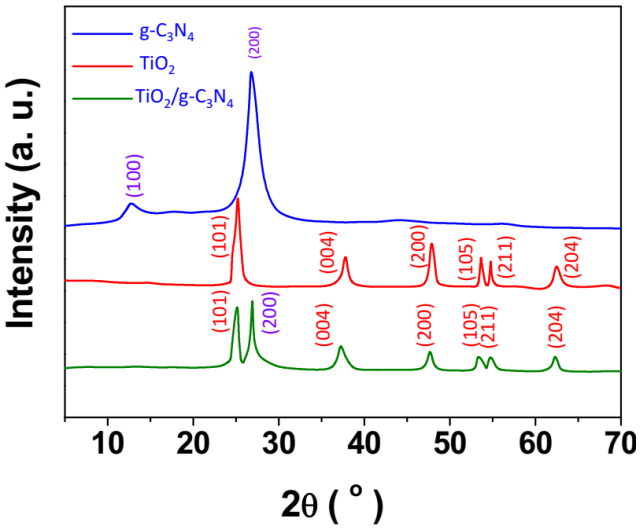

Figure 1. XRD patterns of powders of g-C_3N_4, TiO_2 and TiO_2/g-C_3N_4 hybrid nanocatalysts.

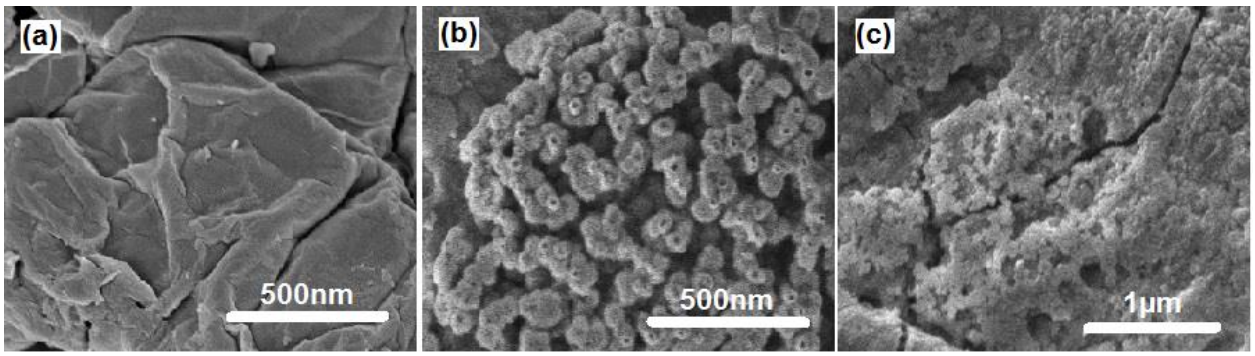

Figure 2. SEM micrographs of (a) g-C_3N_4, (b) TiO_2 and (c) TiO_2/g-C_3N_4 hybrid nanocatalysts.

Figure 2 shows SEM micrographs of g-C_3N_4, TiO_2, and TiO_2/g-C_3N_4 hybrid nanocatalysts. The surface of g-C_3N_4 has a layered sheet structure (Figure 2a). Surface morphology of the sheets is smooth. Figure 2b shows a significant number of irregularly spherical shaped nanoparticles with an average size of 60nm in a SEM micrograph of TiO_2. The hydrothermal-calcination process produces a minor aggregate. TiO_2 nanoparticles are equitably bonded in g-C_3N_4 sheet-like structure, creating heterojunction with high rough and porous hybrid structure, as shown in SEM micrograph of TiO_2/g-C_3N_4 hybrid nanocatalyst. This porosity contains more surface flaws and can increase the effectiveness of light absorption [36, 37].

3.2. Study of optical absorbance spectra

The optical absorbance spectra of g-C_3N_4, TiO_2 and TiO_2/g-C_3N_4 hybrid nanocatalysts are depicted in Figure 3a. It is observed that the spectrum of g-C_3N_4 shows an absorption wavelength up to 450 nm. It is suggested that g-C_3N_4 has good visible light response. Its UV response is lower than that

of TiO_2 [38]. It is in agreement with the reports which indicated that the two-dimensional planar structure of g-C_3N_4 with π-conjugated system benefits the transport of charge carriers, and the narrow bandgap energy with visible-light absorbing ability [39]. Optical absorbance spectra of TiO_2 shows notable absorption edge in the UV region ($\lambda \leq 390$ nm) and poor absorption in the visible light region, which associated with the intrinsic band-gap energy of pure TiO_2 and is indicting to great photocatalytic response to UV light [40-42]. Meanwhile, the TiO_2/g-C_3N_4 hybrid exhibits not only a broader absorption edge than TiO_2 and distinctly enhanced in the visible light region, but also it has the highest optical absorption in comparison to that both of the g-C_3N_4 and TiO_2 nanostructures which can be related to the introduction of Ti^{3+} and the oxygen vacancies [43]. It is reported that introduction of Ti^{3+} and oxygen vacancies into the TiO_2 lattice can form local states at the bottom of the conduction band of TiO_2 which results in visible-light absorption performance while eliminating the recombination effect [44-46]. As depicted in Figure 3b, the band-gap energy (E) value can be obtained from the intercept of linear portion of the $(\alpha h\nu)^{1/2}$ versus photon energy ($h\nu$) to the energy axis, where α is the absorption coefficient, h is the Planck's constant (4.1357×10^{-15} eV.s), and ν is the light frequency. The values of band gap energy of g-C_3N_4, TiO_2 and TiO_2/g-C_3N_4 hybrid nanocatalysts are determined at 2.58, 2.88 and 3.16 eV, respectively. Thus, introducing Ti^{3+} and oxygen vacancies can form the local states and a series of discrete energy levels which reduce the edge of the conduction band create a disordered assembly [47]. The g-C_3N_4 in TiO_2/g-C_3N_4 hybrid also creates a new impurity levels by the upshifted of the TiO_2 valence band edge [48]. As results, formation these local states and impurity levels could considerably decrease the forbidden band width of TiO_2, accordingly, decrease of band gap energy in TiO_2/g-C_3N_4 hybrid toward TiO_2 is evidence of facilitation in photo-excitation of charge carries using low energy, which can extend the light absorption spectrum into the visible region, and accelerate the transmission of the photogenerated charge carriers [49-51]. Eventually, it leads to the production of further electron and hole pairs and melioration of the photocatalytic treatment of the pollutants [48, 52].

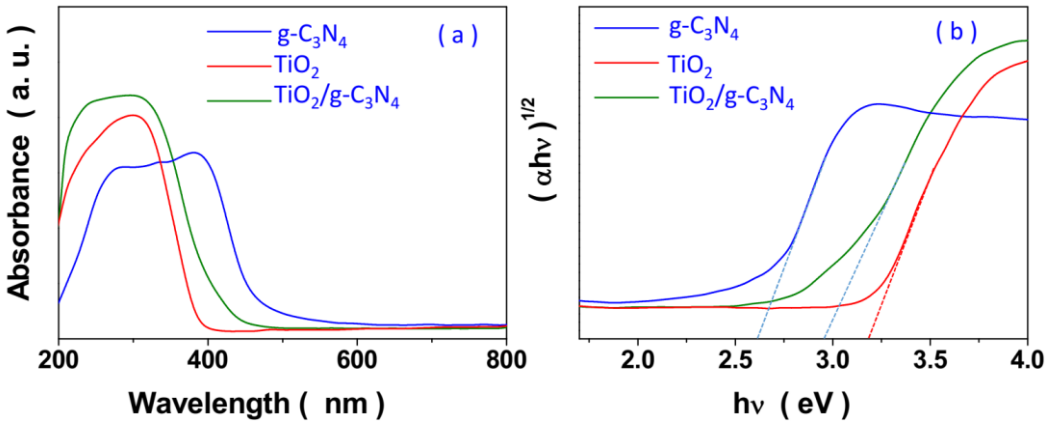

Figure 3. (a) The optical absorbance spectra of g-C_3N_4, TiO_2 and TiO_2/g-C_3N_4 hybrid nanocatalysts and (b) corresponded plots of $(\alpha h\nu)^2$ versus photon energy ($h\nu$).

3.3. Electrochemical analyses

The electrochemical kinetics process in photocatalysts has traditionally been evaluated using EIS experiments. Figure 4 shows Nyquist and Bode diagrams of g-C_3N_4, TiO_2 and TiO_2/g-C_3N_4 hybrid nanocatalysts, respectively. Figure 5 and Table 1 illustrate the equivalent circuit and the acquired parameters by fitting the EIS spectra with the equivalent circuit. The parameters of the corresponding circuit are included. Rct is the first semicircle into the middle-frequency region that is related to charge-transfer resistance and reflects the facility of electron transfer at the electrode/solution interface, and Rs is the series impedance as the nonzero intersection of the semicircle with the real axis at high frequency from the Nyquist plots in Figures 4a [53-55]. Z_N is Nernst diffusion impedance which related to second semicircle at the low-frequency region. C_{dl} presents the chemical capacitance at the interface of photocatalyst/electrolyte. Results indicate that the R_{ct} values of TiO_2/g-C_3N_4 hybrid is remarkably less than pure g-C_3N_4 and TiO_2, implying that merger g-C_3N_4 and TiO_2 provides high porosity and great effective surface area, and more reaction sites to promote the transfer of electrons at the interface of the photocatalyst and electrolyte. As consequence it can enhance the photocatalytic reaction rate [56, 57]. Moreover, the TiO_2/g-C_3N_4 hybrid shows the lowest Z_N value that it is indicated to good diffusion ability in the electrolyte. The depicted Bode plots Figures 4b shows the peak frequency (f_{max}) of TiO_2/g-C_3N_4 hybrid toward g-C_3N_4 and TiO_2 are shifted to low frequency. According to the formula $\tau_n = 1/ (2\pi f_{max})$, f_{max} is inversely related to the electron life time (τ_n). Thereby, the decrease in f_{max} implies an increased electron life time which participates in the electrocatalytic reaction, and a decreased rate for the charge-recombination process for TiO_2/g-C_3N_4 hybrid [58, 59]. These results are in agreement with SEM and optical analyses and confirm the lower charge resistance, an efficient injection of electrons into the TiO_2/g-C_3N_4 hybrid, and its low electron recombination rate which provide the rapid electron transport and higher photodegradation efficiency.

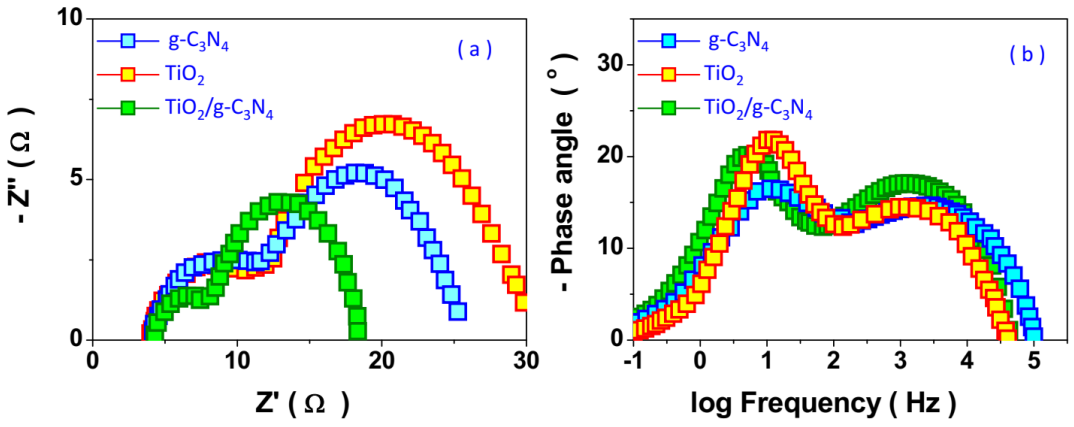

Figure 4. (a) Nyquist and(b) Bode plots of g-C_3N_4, TiO_2 and TiO_2/g-C_3N_4 hybrid nanocatalysts.

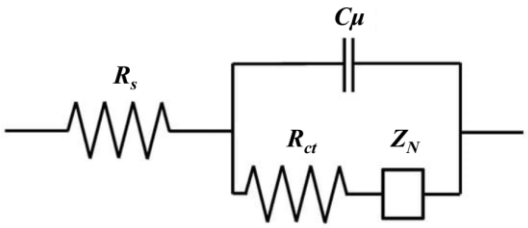

Figure 5. The equivalent circuit.

Table 1. The obtained parameters by fitting the EIS spectra with the equivalent circuit.

Sample	**R_s (Ω)**	**R_{ct} (Ω)**	**Z_N (Ω)**
TiO_2	4.42	5.77	19.28
g-C_3N_4	4.35	2.37	17.20
TiO_2/g-C_3N_4	4.33	1.25	12.09

3.4. Photodegradation activity

Figure 6 shows the findings of a study comparing the photodegradation activities of g-C_3N_4, TiO_2 and TiO_2/g-C_3N_4 hybrid photocatalysts for the treatment of 100 ml of 25 mg/L 2-CP solution to degradation in a control sample without photocatalyst and photodegradation activity in the dark. As can be shown, control sample degradation efficiencies in the dark (first hour) and under solar illumination (for 130 minutes) are 0.09% and 0.8%, respectively. For all photocatalysts, the degradation efficiency after one hour in darkness reaches ≤ 0.9%, and it is drastically increased under solar illumination in first minutes. Accordingly, the degradation efficiency is obtained at 12%, 15% and 25% using g-C_3N_4, TiO_2 and TiO_2/g-C_3N_4 hybrid nanocatalysts after 5 minutes of solar illumination, respectively. These observations confirm the great photocatalytic activity ofg-C_3N_4, TiO_2 and TiO_2/g-C_3N_4 hybrid nanocatalysts under solar illumination [60]. Furthermore, Figure 6 also shows that total degradation of 2-CP is obtained after 125, 110 and 65 minutes of solar illumination in the presence of g-C_3N_4, TiO_2 and TiO_2/g-C_3N_4 hybrid nanocatalysts, respectively. Therefore, the TiO_2/g-C_3N_4 hybrid nanocatalyst illustrates a faster degradation rate of 2-CP than that g-C_3N_4 and TiO_2 which is associated with three factors in good agreement with SEM,EIS and optical analyses: (i) its larger effective surface area and further active sites for photocatalytic processes [61], (ii) more efficient photo-generated electron-hole separation and quick charge transfer than g-C_3N_4 and TiO_2, (iii) its narrow band-gap which can explain the improved photocatalytic elimination of 2-CP under solar illumination.

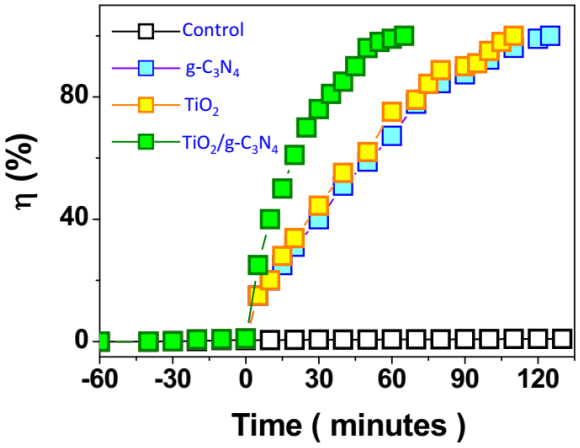

Figure 6. Degradation efficiency of g-C_3N_4, TiO_2 and TiO_2/g-C_3N_4 hybrid photocatalysts for the treatment of 100 ml of 25 mg/L 2-CP solution in dark and under solar irradiation.

Equations 3 to 8 demonstrate the photocatalytic reaction mechanisms for degradation of 2-CP under solar illumination [62, 63]. First, the electron and hole pairs are created on TiO_2/g-C_3N_4 under solar irradiation (Equation 3) in the conduction and valence band, respectively. The electrons are captured by O_2 to form $\bullet O_2^-$ (Equation 4), and further cause the formation of •OH (Equation 6). At the same time, H_2O molecules can be oxidized by photogenerated holes to form •OH (Equation 5). Eventually, 2-CP is degraded by these reactive oxygen species and even mineralized (Equation 7) [64].

TiO_2/g-C_3N_4 + hv → TiO_2/g-C_3N_4 (e^- + h^+) (3)

O_2 + e^- → $\bullet O_2^-$ (4)

H_2O + h^+ → •OH + H^+ (5)

$\bullet O_2^-$ + 2e^- + 2H^+ → •OH + OH^- (6)

2-CP + •OH/$\bullet O_2^-$ → intermediates → products + CO_2 (7)

The effect of initial 2-CP concentrations (10, 25, 50, and 100 mg/L) on TiO_2/g-C_3N_4 hybrid nanocatalyst degrading efficiency was investigated. Figure 7 shows that as the initial 2-CP concentration rises, the degrading effectiveness decreases considerably. Under solar irradiation, total degradation of 10, 25, 50, and 100 mg/L of 2-CP takes 40, 65, 90, and 115 minutes, respectively. Table 2 compares the photocatalytic activity of the photocatalyst in this study to that of various published photocatalysts for the treatment of 2-CP, demonstrating that the TiO_2/g-C_3N_4 hybrid nanocatalyst has a high photocatalytic efficiency due to the creation of intermediate states in the energy band-gap of the hybrid nanocatalyst and efficient separation of electron–hole pairs [65].

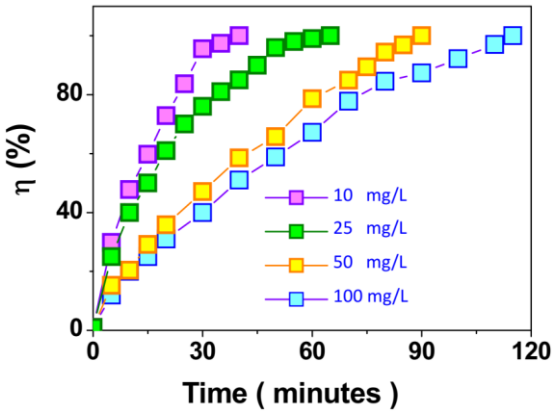

Figure 7. The effect of initial 2-CP concentrations (10, 25, 50 and 100 mg/L) on the degradation efficiency of TiO_2/g-C_3N_4 hybrid nanocatalyst under solar irradiation.

Table 2. Comparison the photocatalytic activity of photocatalyst in this study with that of various reported photocatalysts in the literature for the treatment of 2-CP.

Treatment method	**Material**	**2-CP content (mg/L)**	**Light source**	**Degradation time (minute)**	**η(%)**	**Ref.**
Photocatalyst	TiO_2/g-C_3N_4	10	Solar	40	100	This work
		25		65	100	
		50		90	100	
		100		115	100	
Photocatalyst	TiO_2 (P25)	100	UV	120	95	[66]
Photocatalyst	Ru-doped TiO_2	100	Visible	180	53	[67]
Photocatalyst	ZrO_2-doped $ZnCo_2O_4$	50	Visible	180	91.7	[68]
Photocatalyst	S-doped TiO_2	25	Visible	180	71.4	[69]
Photocatalyst	N-doped TiO_2	25	Visible	150	79.8	[70]
Photocatalyst	Co(III)-doped TiO_2	25	UV	180	93.4	[71]
liquid/solid–ozone	Silica gel	50	---	50	100	[72]
liquid/solid–ozone	Zeolitic	50	---	65	100	[72]
Electrochemical oxidation	Graphite	100	---	20	60	[73]
Electrochemical oxidation	Copper	100	---	20	51.85	[73]
Electrochemical oxidation	Iron	100	---	20	41.90	[73]

The feasibility of using a TiO_2/g-C_3N_4 hybrid nanocatalyst to treat 2-CP in real-world industrial wastewater samples (IWS) was investigated. Under solar irradiation, Figure 8 shows the degrading efficacy of 100mL of 10mg/L 2-CP solution prepared from the actual sample (industrial effluent) and a

control sample (CS) made from deionized water. Total 2-CP treatment takes 40 and 60 minutes in the control sample and industrial wastewater samples, respectively, revealing that total 2-CP treatment takes longer (20 minutes) in industrial wastewater samples due to the presence of inorganic and organic contaminants. However, the results show that the developed photocatalyst is extremely effective at treating 2-CP in industrial effluent [65, 74, 75].

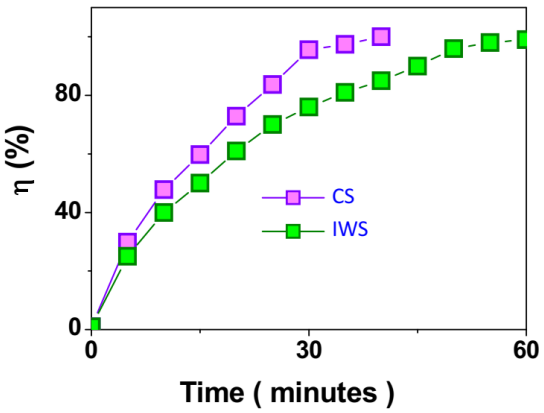

Figure 8. The degradation efficacy of 100mL of 10mg/L 2-CP solution made from actual sample (industrial wastewater) and a control sample made from deionized water under solar irradiation.

4. CONCLUSION

In conclusion, this study described the synthesis of TiO_2/g-C_3N_4 hybrid photocatalysts utilizing a hydrothermal-calcination approach, as well as their use in the degradation of 2-CP as organic water pollutants under solar irradiation. According to structural analysis, the high porosity TiO2/g-C3N4 hybrid nanocatalyst was successfully synthesized. The band gap energies of g-C3N4, TiO_2, and TiO_2/g-C_3N_4 hybrid nanocatalysts were 2.58, 2.88, and 3.16 eV, respectively, according to optical studies. The decrease in band gap energy in TiO_2/g-C_3N_4 hybrid toward TiO_2 was evidence of facilitation in photo-excitation of charge carries using low energy, which can extend the light absorption spectrum into the visible region, hinder the recombination of charges, Electrochemical analysis revealed that the TiO_2/g-C_3N_4 hybrid had a lower charge transfer resistance and a longer electron life time than pure g-C_3N_4 and TiO_2, signifying a low electron recombination rate, allowing for faster electron transport and higher photodegradation efficiency. Total degradation of 2-CP was achieved after 125, 110, and 65 minutes of sun exposure in the presence of g-C_3N_4, TiO_2, and TiO_2/g-C_3N_4 hybrid nanocatalysts, respectively. Because of the production of intermediate states in the hybrid nanocatalyst's energy band-gap and effective separationof electron–hole pairs, the TiO_2/g-C_3N_4 hybrid nanocatalyst demonstrated a high photocatalytic efficiency when compared to several published photocatalysts for the treatment of 2-CP. The practical use of TiO_2/g-C_3N_4 hybrid nanocatalyst to treat 2-CP in genuine industrial wastewater samples (IWS) was studied, and the results revealed the produced photocatalyst's excellent effectiveness in 2-CP treatment in industrial wastewater.

ACKNOWLEDGEMENT
The authors are grateful for the financial support provided by the Natural Science Foundation of Hunan Province (No.2022JJ50263 and No.2021JJ30078).

References

1. T. Apostolović, J. Tričković, M.K. Isakovski, B. Jović, S. Maletić, A. Tubić and J. Agbaba, *Journal of Environmental Sciences*, 98 (2020) 134.
2. W. Liu, F. Huang, Y. Liao, J. Zhang, G. Ren, Z. Zhuang, J. Zhen, Z. Lin and C. Wang, *Angewandte Chemie*, 120 (2008) 5701.
3. A. Zada, M. Khan, M.A. Khan, Q. Khan, A. Habibi-Yangjeh, A. Dang and M. Maqbool, *Environmental Research*, 195 (2021) 110742.
4. L. Zhang, L. Wang, Y. Zhang, D. Wang, J. Guo, M. Zhang and Y. Li, *Environmental research*, 206 (2022) 112629.
5. B. Tang, Z. Yang, Z. Song, G. Shi, D. Fu, X. Sun, J. Zou and H. Qi, *Chemical Engineering Journal Advances*, 8 (2021) 100194.
6. C. Shi, Z. Wu, F. Yang and Y. Tang, *Solid State Sciences*, 119 (2021) 106702.
7. L. Dai, Z. Wang, T. Guo, L. Hu, Y. Chen, C. Chen, G. Yu, L.Q. Ma and J. Chen, *Chemosphere*, 293 (2022) 133576.
8. X. Tian, R. Yang, T. Chen, Y. Cao, H. Deng, M. Zhang and X. Jiang, *Journal of Hazardous Materials*, 426 (2022) 128121.
9. H. Liu, J. Yang, Y. Jia, Z. Wang, M. Jiang, K. Shen, H. Zhao, Y. Guo, Y. Guo and L. Wang, *Environmental Science & Technology*, 55 (2021) 10734.
10. T. Ge, J. Han, Y. Qi, X. Gu, L. Ma, C. Zhang, S. Naeem and D. Huang, *Aquatic toxicology*, 184 (2017) 78.
11. M.-R. Wang, L. Deng, G.-C. Liu, L. Wen, J.-G. Wang, K.-B. Huang, H.-T. Tang and Y.-M. Pan, *Organic letters*, 21 (2019) 4929.
12. Y. Qin, B. Xi, X. Sun, H. Zhang, C. Xue and B. Wu, *Frontiers in Bioengineering and Biotechnology*, 10 (2022) 815.
13. P. Canizares, J. Garcia-Gomez, C. Saez and M. Rodrigo, *Journal of applied electrochemistry*, 33 (2003) 917.
14. L. Feng, X.H. Li, W.C. Lu, Z. Liu, C. Xu, Y. Chen, H.L. Zheng. *International Journal of Biological Macromolecules*, 150 (2020) 617.
15. M. Trapido, A. Hirvonen, Y. Veressinina, J. Hentunen and R. Munter, *The Journal of the International Ozone Association*, 19 (1997) 75.
16. E. Brillas, R. Sauleda and J. Casado, *Journal of the Electrochemical Society*, 145 (1998) 759.
17. M. Barbeni, C. Minero, E. Pelizzetti, E. Borgarello and N. Serpone, *Chemosphere*, 16 (1987) 2225.
18. L. Feng, J.J. Liu, Z.C. Guo, T.Y. Pan, J.H. Wu, X.H. Li, B.Z. Liu and H.L. Zheng, *Separation and Purification Technology*, 285 (2021)120314.
19. M. Khosravi, *Open Access Macedonian Journal of Medical Sciences*, 8 (2020) 553.
20. I.P. Solyanikova and L.A. Golovleva, *Journal of Environmental Science and Health, Part B*, 39 (2004) 333.
21. Y. Nagata, M. Nakagawa, H. Okuno, Y. Mizukoshi, B. Yim and Y. Maeda, *Ultrasonics sonochemistry*, 7 (2000) 115.
22. L. Zhang, Y. Xu, H. Liu, Y. Li, S. You, J. Zhao and J. Zhang, *Journal of Water Process Engineering*, 44 (2021) 102368.
23. J. Tseng and C. Huang, *Water Science and Technology*, 23 (1991) 377.
24. M.M. Ba-Abbad, A.A.H. Kadhum, A.B. Mohamad, M.S. Takriff and K. Sopian, *International Journal of Electrochemical Science*, 7 (2012) 4871.

25. M.M. Ba-Abbad, A.A.H. Kadhum, A.B. Mohamad, M.S. Takriff and R. Jalgham, *International Journal of Electrochemical Science*, 7 (2012) 11363.
26. H. Liu, *International Journal of Electrochemical Science*, 17 (2022) 220322.
27. H. Karimi-Maleh, H. Beitollahi, P.S. Kumar, S. Tajik, P.M. Jahani, F. Karimi, C. Karaman, Y. Vasseghian, M. Baghayeri and J. Rouhi, *Food and Chemical Toxicology*, (2022) 112961.
28. G. Li, X. Nie, J. Chen, Q. Jiang, T. An, P.K. Wong, H. Zhang, H. Zhao and H. Yamashita, *Water research*, 86 (2015) 17.
29. N. Rao, A. Dubey, S. Mohanty, P. Khare, R. Jain and S. Kaul, *Journal of hazardous materials*, 101 (2003) 301.
30. H. Xing, C. An, L. Wu and Y. Xu, *International Journal of Electrochemical Science*, 17 (2022) 220510.
31. H. Azizi-Toupkanloo, M. Karimi-Nazarabad, M. Shakeri and M. Eftekhari, *Environmental Science and Pollution Research*, 26 (2019) 30941.
32. T. Gao, C. Li, Y. Zhang, M. Yang, D. Jia, T. Jin, Y. Hou and R. Li, *Tribology International*, 131 (2019) 51.
33. M. Akbari, R. Moghadam, R. Elmi, A. Nosrati, E. Taghiabadi and N. Aghdami, *Journal of Ophthalmic and Vision Research*, 14 (2019) 400.
34. D. Ge, H. Yuan, J. Xiao and N. Zhu, *Science of The Total Environment*, 679 (2019) 298.
35. M. Ghalandarzadeh and S. Afrang, *International Journal of Engineering*, 34 (2021) 2534.
36. B. Abebe, H.A. Murthy and E. Amare, *Environmental Nanotechnology, Monitoring & Management*, 14 (2020) 100336.
37. L. Tang, Y. Zhang, C. Li, Z. Zhou, X. Nie, Y. Chen, H. Cao, B. Liu, N. Zhang and Z. Said, *Chinese Journal of Mechanical Engineering*, 35 (2022) 1.
38. S. Zhao, S. Chen, H. Yu and X. Quan, *Separation and Purification Technology*, 99 (2012) 50.
39. Q. Sun, K. Lv, Z. Zhang, M. Li and B. Li, *Applied Catalysis B: Environmental*, 164 (2015) 420.
40. V. Etacheri, C. Di Valentin, J. Schneider, D. Bahnemann and S.C. Pillai, *Journal of Photochemistry and Photobiology C: Photochemistry Reviews*, 25 (2015) 1.
41. X. Wu, C. Li, Z. Zhou, X. Nie, Y. Chen, Y. Zhang, H. Cao, B. Liu, N. Zhang and Z. Said, *The International Journal of Advanced Manufacturing Technology*, 117 (2021)
42. H. Karimi-Maleh, C. Karaman, O. Karaman, F. Karimi, Y. Vasseghian, L. Fu, M. Baghayeri, J. Rouhi, P. Senthil Kumar and P.-L. Show, *Journal of Nanostructure in Chemistry*, (2022) 1.
43. L. Shen, Z. Xing, J. Zou, Z. Li, X. Wu, Y. Zhang, Q. Zhu, S. Yang and W. Zhou, *Scientific Reports*, 7 (2017) 41978.
44. K. Li, S. Gao, Q. Wang, H. Xu, Z. Wang, B. Huang, Y. Dai and J. Lu, *ACS applied materials & interfaces*, 7 (2015) 9023.
45. T. Gao, Y. Zhang, C. Li, Y. Wang, Q. An, B. Liu, Z. Said and S. Sharma, *Scientific reports*, 11 (2021) 1.
46. R. Rahmi, S. Lubis, N. Az-Zahra, K. Puspita and M. Iqhrammullah, *International Journal of Engineering*, 34 (2021) 1827.
47. S. Zhou, S. Liu, K. Su and K. Jia, *Journal of Alloys and Compounds*, 804 (2019) 10.
48. M.-Y. Yan, Z.-Y. Jiang, J.-M. Zheng, Y.-M. Lin and Z.-Y. Zhang, *Applied Surface Science*, 531 (2020) 147318.
49. P. Devaraji and C.S. Gopinath, *International Journal of Hydrogen Energy*, 43 (2018) 601.
50. Q. Li, L. Zong, Y. Xing, X. Wang, L. Yu and J. Yang, *Science of Advanced Materials*, 5 (2013) 1316.
51. M. Khosravi, *European journal of translational myology*, 31 (2021) 9411.
52. X. Bi, S. Yu, E. Liu, L. Liu, K. Zhang, J. Zang and Y. Zhao, *Colloids and Surfaces A: Physicochemical and Engineering Aspects*, 603 (2020) 125193.

53. F. Pogacean, M. Ştefan, D. Toloman, A. Popa, C. Leostean, A. Turza, M. Coros, O. Pana and S. Pruneanu, *Nanomaterials*, 10 (2020) 1473.
54. H. Karimi-Maleh, R. Darabi, M. Shabani-Nooshabadi, M. Baghayeri, F. Karimi, J. Rouhi, M. Alizadeh, O. Karaman, Y. Vasseghian and C. Karaman, *Food and Chemical Toxicology*, 162 (2022) 112907.
55. E. Darezereshki, A. Behrad Vakylabad and M. Yousefi, *International Journal of Engineering*, 34 (2021) 1888.
56. S. Tu, Y. Guo, Y. Zhang, C. Hu, T. Zhang, T. Ma and H. Huang, *Advanced Functional Materials*, 30 (2020) 2005158.
57. H. Li, Y. Zhang, C. Li, Z. Zhou, X. Nie, Y. Chen, H. Cao, B. Liu, N. Zhang and Z. Said, *The International Journal of Advanced Manufacturing Technology*, 120 (2022) 1.
58. M.P.A. Muthalif and Y. Choe, *Applied Surface Science*, 508 (2020) 145297.
59. H. Maleh, M. Alizadeh, F. Karimi, M. Baghayeri, L. Fu, J. Rouhi, C. Karaman, O. Karaman and R. Boukherroub, *Chemosphere*, (2021) 132928.
60. J. Rouhi, H.K. Malayeri, S. Kakooei, R. Karimzadeh, S. Alrokayan, H. Khan and M.R. Mahmood, *International Journal of Electrochemical Science*, 13 (2018) 9742.
61. W. Wang, J. Fang, S. Shao, M. Lai and C. Lu, *Applied Catalysis B: Environmental*, 217 (2017) 57.
62. F. Li, P. Du, W. Liu, X. Li, H. Ji, J. Duan and D. Zhao, *Chemical Engineering Journal*, 331 (2018) 685.
63. A. Zada, Y. Qu, S. Ali, N. Sun, H. Lu, R. Yan, X. Zhang and L. Jing, *Journal of hazardous materials*, 342 (2018) 715.
64. L. Nan, C. Yalan, L. Jixiang, O. Dujuan, D. Wenhui, J. Rouhi and M. Mustapha, *RSC Advances*, 10 (2020) 27923.
65. H. Li, Y. Zhang, C. Li, Z. Zhou, X. Nie, Y. Chen, H. Cao, B. Liu, N. Zhang and Z. Said, *Korean Journal of Chemical Engineering*, 39 (2022) 1107.
66. N.N. Rao, A.K. Dubey, S. Mohanty, P. Khare, R. Jain and S.N. Kaul, *Journal of Hazardous Materials*, 101 (2003) 301.
67. R.A. Elsalamony and S.A. Mahmoud, *Arabian Journal of Chemistry*, 10 (2017) 194.
68. J. Rashid, M. Barakat, R. Mohamed and I. Ibrahim, *Journal of Photochemistry and Photobiology A: Chemistry*, 284 (2014) 1.
69. N. Sharotri and D. Sud, *New Journal of Chemistry*, 39 (2015) 2217.
70. N. Sharotri and D. Sud, *Desalination and Water Treatment*, 57 (2016) 8776.
71. M. Barakat, H. Schaeffer, G. Hayes and S. Ismat-Shah, *Applied Catalysis B: Environmental*, 57 (2005) 23.
72. C. Tizaoui, R. Bickley, M. Slater, W. Wang, D. Ward and A. Al-Jaberi, *Desalination*, 227 (2008) 57.
73. M.S. Ullah, A.U.R. Majid, U. Zahid, G. Abbas, Y. Shahid and A. Maroof, *Kocaeli Journal of Science and Engineering*, 1 (2018) 42.
74. U. Saindane, S. Soni and J. Menghani, *International Journal of Engineering*, 34 (2021) 2517.
75. C. Liu and J. Rouhi, *RSC Advances*, 11 (2021) 9933.